Final Draft
Manuscript available at: https://doi.org/10.1061/(ASCE)ST.1943-541X.0001537
Full citation: Ballard, ZC, Gerbo, EJ, Thrall, AP, and Smith, BJ (2016) "Behavior of Sandwich Panels in a Deployable Structure." Journal of Structural Engineering, 142(10), 04016073

Behavior of Sandwich Panels in a Deployable Structure

Zach C. Ballard, [1]; Evan J. Gerbo, S.M.ASCE [2]; Ashley P. Thrall, A.M.ASCE [3]; Brian J. Smith, P.E. [4];

ABSTRACT

This paper investigates the load-bearing capability of sandwich panels (comprised of fiber-reinforced polymer faces and a foam core) connected by aluminum hinges in an origami-inspired deployable structure intended for temporary sheltering. The structure is studied (1) during deployment (loaded under self-weight only), and (2) as both individual and combined modules subjected to uniform pressures emulating wind loads. The measured results are used to validate finite element models, with comparisons focusing on surface strains and displacements at panel centers (to study global behavior), as well as surface strains near connections (to study local behavior). The validated numerical models are used to perform parametric studies investigating design decisions for (1) deployment, including panel reinforcement, location of lifting equipment, and size of lifting equipment, and (2) combined modules, including restraints and connections between modules, gasketing between panels, and panel reinforcement. This research ultimately demonstrates the load-bearing capability of deployable structures comprised of hinged sandwich panels and provides design guidelines and recommendations.

CE Database subject headings: Temporary structures; Sandwich panels; Military engineering

INTRODUCTION AND MOTIVATION

The behavior of sandwich panels (i.e., layered material comprised of a core and two faces)

[1]Postdoctoral Research Associate, Kinetic Structures Laboratory, Department of Civil and Environmental Engineering and Earth Sciences, University of Notre Dame, 228 Cushing Hall, Notre Dame, IN 46556. E-mail: zballard@nd.edu

[2]Graduate Student, Kinetic Structures Laboratory, Department of Civil and Environmental Engineering and Earth Sciences, University of Notre Dame, 228 Cushing Hall, Notre Dame, IN 46556. E-mail: egerbo@nd.edu

[3]Myron and Rosemary Noble Assistant Professor of Structural Engineering, Kinetic Structures Laboratory, Department of Civil and Environmental Engineering and Earth Sciences, University of Notre Dame, 159 Fitzpatrick Hall, Notre Dame, IN 46556. (corresponding author) E-mail: athrall@nd.edu

[4]Assistant Teaching Professor and Research Engineer, Kinetic Structures Laboratory, Department of Civil and Environmental Engineering and Earth Sciences, University of Notre Dame, 228 Cushing Hall, Notre Dame, IN 46556. E-mail: bsmith24@nd.edu

has been widely studied since the 1960s, with applications ranging from aerospace to shipping industries. Due to the high strength-to-weight ratio and the thermal insulation provided by the core, sandwich panels can be particularly advantageous for implementation in temporary sheltering in military or disaster relief applications where transportability and energy efficiency in heating and cooling are at a premium [e.g., 66 million USD is spent per day by the U.S. military to cool soft wall (i.e., canvas) shelters (Anderson, 2011)] (Martinez-Martin and Thrall, 2014; Quaglia et al., 2014b). To make these structures deployable, origami can be utilized for inspiration to fold panels along hinged connections [see Peraza-Hernandez et al. (2014)].

Quaglia et al. (2014a) proposed a solution for an origami-inspired deployable shelter (Figure 1) comprised of hinge-connected sandwich panels [fiber-reinforced polymer (FRP) faces and a foam core] that includes the advantages of existing military soft wall (i.e, deployability, low self-weight) and rigid wall (i.e., insulation) shelters (Quaglia et al., 2014b). This four-panel concept (back wall, roof, and two wing walls) folds into a compact shape for transportation by air, rail, ship, or truck on a standard military pallet [463L pallet, Compliance Packaging International Ltd. (2013)]. It can be deployed (Figure 1a) without heavy lifting equipment using a lever arm that enables users to rotate the back wall about a fulcrum. The wing walls and roof are then rotated out to form a fully deployed, self-supporting module. Modules can be mated (Figure 1b) and combined with other modules and existing technologies [e.g., kichens, latrines housed in Tricon containers (Charleston Marine Containers, Inc., 2011) in the current Force Provider system (United States Army Integrated Logistics Support Center Natick, 2013)] to form larger shelters (Figure 1c). A full-scale prototype of this system (Figure 1d) has been demonstrated.

However, a barrier to the implementation of deployable folding structures is a knowledge gap in the behavior of structures comprised of multiple sandwich panels that act as the primary load-bearing components. Prior experimental research has primarily focused on isolated sandwich panels, including understanding the flexural [e.g., Manalo et al. (2010), Abbadi et al. (2009), Kesler and Gibson (2002), Daniel and Abot (2000), Kee Paik et al. (1999)] and compressive [e.g, Malcom et al. (2013), Mamalis et al. (2005), Kee Paik et al. (1999)] behavior, as well as failure modes [e.g., Russo and Zuccarello (2006)]. Experimental and numerical research has also been performed on fasteners/inserts of sandwich panels [e.g., Heimbs and Pein (2009), Bunyawanichakul et al. (2005), Demelio et al. (2001), De Matteis and Landolfo (1999a)]. A few exceptions have investigated multi-panel structures [e.g., Dawood and Peirick III (2013), Heimbs and Pein (2009), De Matteis and Landolfo (1999a), and De Matteis and Landolfo (1999b)]; however, these studies did not investigate foldable or deployable structures featuring hinged connectors. To address the existing knowledge gap related to multi-panel structures, this paper builds off of a previous study by the authors focused on an isolated panel restrained by hinged connectors (Ballard et al., 2016) and investigates the load-bearing capability of sandwich panels (FRP faces and foam core) connected by aluminum hinges in a multi-panel structure.

OBJECTIVES AND SCOPE

The objectives of this research are to study (1) the impact of deployment on panel behavior and (2) the load-bearing behavior of individual and combined modules across hinged connections for the structure shown in Figure 1. During deployment, the behavior of the back wall was monitored as the half-scale structure rotated into the deployed position. The behaviors of half-scale individual and combined modules were studied under increasing uniformly distributed surface pressures that emulate wind loading. For each test, the measured results are compared with finite element numerical models to better understand the global structural behavior of the shelter as well as local effects near boundary conditions and panel connections. Parametric studies using the resulting validated numerical models investigate design decisions for (1) deployment, including panel reinforcement, location of lifting equipment, and size of lifting equipment, and (2) combined modules, including restraints and connections between modules, gasketing between panels, and panel reinforcement. This research demonstrates the load-bearing capability of sandwich panels connected by aluminum hinges and culminates in design guidelines and recommendations.

MATERIAL PROPERTIES

Table 1 provides the measured material properties of the FRP face and foam core of the sandwich panel. The FRP faces [1.78 mm (0.07 in.) thick] are Vectorply biaxial (E-LT 1200-P) and double-bias (E-BX 1200) e-glass laminate (layup: 0°/90°/45°/-45°/-45°/45°/90°/0°) (Vectorply, 2002) with vinyl ester resin. The core [31.8 mm (1.25 in.)] is Corecell M80 Foam (Gurit, 2013). Material samples were manufactured by Lyman-Morse Boatbuilding Co. (Thomaston, ME). Individual samples of the core, face, and sandwich panel were used during testing (Figure 2). All material tests were conducted according to the applicable ASTM standards using an Instron 5590 Universal Testing Machine. Data from this material testing was previously used by the authors to investigate the behavior of an isolated panel (Ballard et al., 2016).

The core (Figure 2a) was tested to determine the core density, ρ_c per ASTM C271 (ASTM, 2011a) as well as the core compressive modulus, E_c and core ultimate strength, σ_c per ASTM C365 (ASTM, 2011b). The FRP was tested to determine the face density, ρ_f per ASTM D792 (ASTM, 2013) as well as the face tensile modulus, E_f, face Poisson's ratio, ν_f and face ultimate strength, σ_f per ASTM D3039 (ASTM, 2008). Two different FRP face samples were used: a standard straight sample (Figure 2b) used to determine E_f and ν_f and a dog-bone sample (Figure 2c) used to determine σ_f. The dog-bone sample was designed to promote failure in the gage (or center) region of the sample (required per ASTM D3039) as used in ASTM D638 (ASTM, 2010) with a radii as recommended by El-Chiti (2005). The strain values required for calculating ν_f were obtained using strain gages (MicroMeasurements CEA-00-250UW-350) adhered near the failure region of the samples. The sandwich panel (Figure 2d) was tested to determine the shear strength of the core, τ_c per ASTM C393 (ASTM, 2011c) and the core shear modulus, G_c per ASTM D7250 (ASTM, 2012).

EXPERIMENTAL PROGRAM

A half-scale prototype of the shelter in Figure 1 is tested under three different conditions:

- Deployment: shelter was rotated to erect position (Figure 3).
- Individual Module: Modules A and B were loaded individually under increasing uniformly distributed surface loads (Figure 4a, 4b, 4d, and 4e).
- Combined Modules: Modules A and B were joined and loaded under increasing uniformly

distributed surface loads (Figure 4g and 4h).

Dimensions of the modules are provided in Figures 4 and 5. Note that these are the idealized dimensions based on the initial design and do not include construction tolerances that result in slight differences [on the order of 3.18 mm (0.125 in)]. Thickened panel edges (i.e., end caps, shown in Figure 4) increase the FRP thickness from 1.78 mm (0.07 in.) to 4.95 mm (0.195 in). There is also a thickened FRP reinforcement region [4.95 mm (0.195 in) thick] that is 305 mm (12.0 in) in length along the back wall to support the attachment of the lever arms (Figure 3b). The back wall is connected to each wing wall by three aluminum (alloy type 5052) hinges (Detail A, Table 2) spaced approximately equidistant along each edge (Figure 4c and 5). A continuous hinge (Detail B, Table 2) connects the back wall to the roof (Figure 4f and 5). Gasketing (Detail C, Table 2) is placed between panels (i.e., at back wall - roof, roof - wing wall, and wing wall - back wall interfaces) for insulation and water tightness. The lever arm has a diameter of 63.5 mm (2.50 in) with a thickness of 3.18 mm (0.125 in).

When deployed, each module was anchored to the ground at four locations (Figure 4). Each wing wall was restrained to the floor by an aluminum angle (Detail D, Table 2). Two fasteners [6.35 mm (0.250 in) diameter steel] connected the angle to the wing wall and a single bolt [6.35 mm (0.250 in) diameter steel] anchored the angle to the floor (Figure 4j). The back wall was restrained to the floor by an extended FRP flange (Detail E, Table 2). Two bolts [6.35 mm (0.250 in) diameter steel] anchored this flange to the floor (Figure 4j). The wing walls and roof were connected by aluminum angles (Detail F, Table 2). One leg was fastened to the roof [two fasteners, 6.35 mm (0.250 in) diameter steel] and the other leg was attached to the wing wall by clamps (Figure 4k). Modules were joined by clamps at the top of the roof panels (Figure 4l).

Deployment Test

For the deployment test, the folded structure was manually rotated from an initial deployment angle, θ (measured using a Measurement Specialties Accustar I Series clinometer), of 0 ° (i.e., back wall is parallel to the ground) to a final angle of 75° (i.e., fully erect) using a three-pronged lever arm (Figure 3). A range of different hand positions on the lever arm were investigated (shown in Figure 3c). Only the surface strains of the back wall were measured (using 10 MicroMeasurements N2A-00-10CBE-350 strain gages adhered to the tension side of the panel, Figure 3b) since the lever arm was directly connected to the back wall and the other panels were essentially unloaded during the deployment process.

Individual/Combined Module Tests

In the individual and combined module tests (Figure 4), back wall and roof panels were subjected to an increasing uniformly distributed pressure [up to 2.39 kPa (50 psf)]. The direction of the pressures was determined to emulate design wind loads per ASCE/SEI 7-10 design standards (ASCE, 2010) (windward direction against back wall of Module B, positive internal pressure coefficient, negative external roof pressure coefficients). Modules A and B (identified in Figure 4) were each tested independently and then as a combined system. In individual module tests, pressure was applied to (1) only the back wall, (2) only the roof, and (3) both back wall and roof simultaneously. In the combined module tests, pressure was applied to the (1) back wall and roof of Module A, (2) back wall and roof of Module B, and (3) back wall and roof of both Modules A and B.

The pressure loads were applied using urethane film air bladders attached to a rigid, steel reaction frame anchored to the floor (Figure 4). The magnitude of pressure in each bladder was measured using a pressure sensor (Omega PX409) connected by air tubes. Throughout the paper, the reported "applied pressure" refers to the pressure above that when the bladders makes full contact [at 0.96 kPa (20.0 psf)]. Strains and displacements were reported accordingly. This does not include the effects of self-weight and strains/displacements induced during uneven bladder inflation before full contact (as the amount of bladder contact could not be measured or numerically simulated prior to full contact). Longitudinal and transverse surface strains on all panels were measured (using up to 80 strain gages MicroMeasurements N2A-00-10CBE-350, MicroMeasurements EA-13-10CBE-120/E), while horizontal and vertical panel displacements were measured using displacement transducers (MD Totco 1850-002, hereafter string pots) attached to stationary supports (Figure 5). Note that "S" identifies string pots, "O" indicates strain gages on the outside surface of the structure, and "I" indicates strain gages on the inside surface. Labels "A" and "B" indicate measurements made on Module A and Module B, respectively.

NUMERICAL MODELING

Three-dimensional finite element models were created in ABAQUS (ABAQUS, 2013). The panels were modeled using S4R shell elements for the panel faces and C3D8R solid elements for the core, with linear-elastic stress-strain relationships based on the properties from material testing (Table 1). The face elements were continuously tied to the core. The hinges connecting panels were approximated as hinge leaves connected at the barrel location through constraints that permit free rotation, but restrained relative translation. The hinge leaves were modeled as S4R shell elements using the Aluminum design code (The Aluminum Association, 2005) specified material properties for aluminum [alloy type 5052; assumed material properties: E=70.330 MPa (10,200 ksi), ρ=2680 $\frac{kg}{m^3}$ (168 $\frac{lb}{ft^3}$)]. Connections between leaves and panels were modeled as continuous ties along the shell face elements. For all components, a maximum mesh size of 12.7 mm (0.5 in) was used for numerical convergence.

This modeling approach was previously validated by the authors (Ballard et al., 2016). In this prior work, an isolated sandwich panel, comprised of the same materials, was subjected to a uniform load and restrained by hinged connectors. The measured global behavior (strains and displacements at the panel center) and local behavior (strains near hinged connectors) very closely matched numerical predictions, justifying the use of the same numerical modeling approach for this new study.

Deployment Test

Deployment was captured quasi-statically by making separate models at deployment angles of θ = 5 °, 20 °, 40 °, 60 °, and 75 °. The lever arm was modeled as aluminum C3D8R solid elements and as solid 63.5 mm (2.50 in) thick cylinders for simplicity. It was continuously tied to the outer face shell elements of the back wall. Boundary conditions include pin restraints (i.e., translation restrained, free rotation) along the full length of the inner bottom edge of the back wall that acts as the fulcrum. Pin restraints were also placed along the restraint edge of the lever arm, emulating the restraint of people implementing the lever arm (Figure 3). Only self-weight is considered during deployment. The contact and interaction between panels is critical to model as the back wall supports the wing walls and roof during deployment. In the experiment, a strap secures the wing walls so that they lie effectively perpendicular to the back wall during deployment. This is modeled numerically by restraining the rotation at the wing wall-back wall hinges. In the experiment, the roof contacts the wing wall only at two small areas [76.2 mm (3 in) by 25.4 mm (1 in) each] where foam inserts were added to achieve a gap between the roof and the wing wall which was need to protect the strain gages. In the numerical model, a frictionless contact surface was modeled between the roof and back wall only in these regions. The roof-back wall hinge was free to rotate.

Individual/Combined Module Tests

The roof-wing wall connections (Figure 4k) were approximated as an aluminum angle modeled as C3D8R solid elements. Surfaces of the angle were continuously tied to the shell face elements of the roof and wing wall. Gasketing between panels was modeled using 6.35 mm (0.25 in) thick C3D8R solid elements and as an essentially incompressible material for simplicity. The roof-to-roof connection (Figure 4l) at the ridge of the two module structure was approximated by constraining relative horizontal translation along the bottom edge of the roof panels between modules (in the direction of applied pressure).

To achieve realistic boundary conditions, the structure was modeled as bearing on a rigid, frictionless surface. The wing wall restraint (Figure 4j) was approximated by modeling an aluminum angle (C3D8R solid elements) that was continuously tied to the wing wall shell face elements on the vertical leg. On the horizontal leg, fixed restraints (i.e., translation and rotation restrained) were implemented on the top surface of the angle at the approximate location of the hex nut securing the bolt. The angle also bears on the rigid, frictionless surface. The back wall restraint flange (Figure 4j) was modeled as S4R shell elements and extends from the inner face of the back wall outward, bearing on the rigid, frictionless surface and tied to the core at the panel base. Fixed restraints were implemented (similarly to the wing wall restraint) at the approximate locations of the hex nuts securing the two flange bolts.

BEHAVIOR DURING DEPLOYMENT

A challenge in the design of deploying structures is ensuring good structural performance during deployment (typically under self-weight) and when fully deployed (under service loads) while still meeting priorities related to a low self-weight and a small packaged volume. In the structure investigated in this study (Figure 1), the packaged structure acts as a cantilever beam in Stage I of deployment and transitions to column behavior by the end of Stage III (Figure 3a). Further, high stress concentrations may result during deployment near the lever arm attachment. Therefore, an engineer must design for not only different loading conditions, but also to behave as different structural systems.

To better understand the behavior during deployment, the structure was monitored as the back wall was rotated into its fully erect position. The measured results were compared to numerical models for the varying hand placements (Figure 3c) considered to understand the impact of the deployment implementation on behavior (i.e., studying the effect of varying soldier force placement on behavior since field implementation is unpredictable). The resulting validated numerical models were used to perform parametric studies aimed at understanding the impact of (1) panel reinforcement along the back wall, (2) location of lifting equipment (i.e., number of lever arm attachment points), and (3) size of lifting equipment (i.e., diameter of the lever arm).

Deployment Test

Figure 6 compares the measured and numerical behavior of the back wall at Locations A-J (Figure 3b) as a function of the deployment angle. Note that positive strains refer to tension and negative strains refer to compression. Three sets of measured data are included corresponding to the hand placement depicted in Figure 3c. This is compared with numerical models with pinned restraints along the lever arm approximating hand placement (i.e., “center” refers to restraints along the full length of restraint edge of the lever arm, “left” refers to restraints along the left half of the restraint edge, “right” refers to restraints along the right half). Locations for data comparison were selected to capture the global behavior (e.g., Loc. A is the center of panel) and local behavior - including the end of the thickened reinforcement region (Loc. B-G) and near the lever arm attachment (Loc. H-J) on left, center, and right sides of the back wall.

The global behavior of the back wall (Loc. A) indicates that the back wall acted as a cantilever at low angles of deployment in Stage I, with high tensile strains corresponding to low deployment angles. It transitioned to column-like behavior by Stage III, where strains became slightly compressive. The numerical predictions match the measured data very closely. There is negligible difference in behavior for varying hand positions in either the measured or numerical results.

Considering the local behavior at the panel midline (Loc. C, F, and I), the numerical models are able to closely predict the measured strains. Again, there is negligible difference between results for varying hand placement. As expected, there is a sharp increase in strain where the thickened reinforcement region ends. Within this thickened reinforcement region, strains were highest near the lever arm attachment (Loc. I).

There is a large discrepancy between the measured strains in the left side of the panel (Loc. B, E, and H) and the right side of the panel (Loc. D, G, and J), with the left side exhibiting significantly larger measured strains than the right. The numerical models significantly under-predict the strains in the left, while closely matching the strains on the right. These differences can be attributed to the fit of the lever arm in the attachment holes. It was observed that the left lever arm prong fit much tighter in its hole than the right lever arm prong. This resulted in an unbalanced application of force during deployment, resulting in larger measured strains in the left region.

While the impact of hand placement had a negligible effect along the midline of the back wall, there is a significant difference in behavior locally on the left (Loc. B, E, and H) and on the right (Loc. D, G, and J). As expected, when hands are placed on the left, larger strains were observed in the measured and numerical data on the left side of the panel and lower strains on the right. The opposite effect is observed with hands placed on the right. Since field conditions are unpredictable and an unbalanced force may be applied to the lever arm, a designer must consider an envelope of behaviors as shown here. Further experimental studies were performed related to the distance between hands placed on the level arm (i.e., two hands very close or very far apart); however, the results of these studies showed negligible impact on panel behavior.

Overall, the comparisons between numerical and measured data validated the models, allowing the models to be used for parametric studies aimed at understanding the impact of design decisions.

Parametric Study of Panel Reinforcement, Location of Lifting Equipment, and Size of Lifting Equipment

To understand the impact of (1) panel reinforcement along the back wall, (2) number of lever arm attachment points, and (3) diameter of the lever arm on behavior, parametric studies were performed using the validated numerical models (Figure 7). All results are shown for a deployment angle of $\theta = 5\,^\circ$ since this is the most critical scenario (i.e., resulting in the larger surface strains). Strains are shown as a function of panel location where 0 refers to the bottom of the panel. Results are shown up to a distance of 500 mm (19.7 in, or approximately 40$\%$ of the panel length) to focus on the most critical regions.

As discussed earlier, the length of the thickened reinforcement region is critical for design as strains significantly increase where this region ends. Minimizing the length of this region can reduce cost and weight. Figure 7a shows the numerical longitudinal surface strains along the midline of the panel for the prototype [featuring a 305 mm (12.0 in) long reinforcement region] and for a structure with a reduced length of the reinforcement region [152 mm (6.00 in)]. From the bottom of the panel to 152 mm (6.00 in), the two models are effectively the same. Within the lever arm region (shaded in grey), strains are compressive on the lower side and highly tensile on the upper side, as expected. Each numerical model shows an increase in tensile strain at its respective end of the reinforcement region of approximately the same magnitude, with the models agreeing again after 305 mm (12.0 in). This shows negligible global impact in shortening the reinforcement region. For each model, the largest strain is located directly in line with the upper edge of the lever arm, with a drastic strain reduction at a small distance away from the lever arm. Therefore, the reinforcement region could be terminated much closer to the lever arm attachment. A design recommendation is to limit the reinforcement region to just beyond the attachment location.

The lever arm for the prototype structure was designed to have three prongs attached to the back wall to distribute the localized effects of attachment. However, reducing the number of prongs to two (i.e., an attachment at left and right only with the center prong removed) would reduce the weight of the lever arm as well as cost in manufacturing. To investigate the impact of reducing the number of attachment points, Figure 7b shows numerical strain at the (1) midline with three attachments, (2) midline with two attachments, (3) left (i.e., along line of left-most attachment) with three attachments, and (4) left with two attachments. As expected, the midline strains for the two attachment model do not exhibit the increases in compressive/tensile strains where the lever arm would have attached. However, at the left of the panel, these spikes are significantly larger than those for the three attachment model. Overall, there is a tradeoff in increased local strains for a reduction in the number of lever arm prongs/attachments. A designer would need to weigh the advantages and disadvantages of this effect in relation to weight and cost of the structure.

Reducing the diameter of the lever arm can reduce weight and cost. Figure 7c shows a numerical comparison between the behavior of the prototype [63.5 mm (2.5 in) diameter lever arm] and a structure with a reduced diameter lever arm [31.8 mm (1.25 in) diameter]. The dashed grey lines indicate the outline of the reduced lever arm. There is negligible difference in behavior near the bottom of the panel [after approximately 150 mm (5.91 in)]. However, the 31.8 mm (1.25 in) diameter lever arm model shows significantly larger tensile strains at the edge of the lever arm. Therefore, a designer should evaluate the additional cost/weight of reinforcement in this region compared to the savings in lever arm diameter.

BEHAVIOR OF INDIVIDUAL AND COMBINED MODULES

To characterize the behavior of the structure, back wall and roof panels of the module were subjected to an increasing uniformly distributed pressure [up to 2.39 kPa (50 psf)]. The results were compared against numerical predictions, culminating in validated numerical models. The validated models were used to perform parametric studies to investigate the impact of the (1) restraints and the connection between modules, (2) gasketing between panels, and (3) panel end cap reinforcement.

Module A Test

Figure 8 shows the measured and numerical deformed shape (deformations magnified by a factor of 75) and Figure 9 shows the measured and numerical strains at panel centers under pressures applied to the back wall, the roof, and both the roof and back wall of Module A. When only the back wall was loaded, the back wall both rotates backward (captured numerically and measured at Loc. SA 1) and also bends (shown numerically) (Figure 8a). The measured strains at the center of the back wall (Loc. AO 1) increase linearly with pressure and match numerical predictions well (Figure 9a). However, the measured displacements at the top of the roof (Loc. AS 3) show that the roof is tilting slightly downward while the numerical models predict that it remains approximately parallel to its original undeformed shape. This discrepancy can be attributed to the "play" in the hinge connecting the back wall to the roof. It was observed that the hinge leaves can translate relative to one another as well as rotate. While this relative movement within the hinge itself is very small, it does impact the measured results and is evident when just the roof was loaded (Figure 8b), as Loc. AS 2 under-translates while Loc. AS 3 over-translates in comparison to the numerical model. The play in the hinges effectively results in a different angle of rotation between the back wall and the roof. This is further shown when both the back wall and roof were loaded (Figure 8c). Nevertheless, the numerical models were able to reasonably predict the strains at the center of the back wall and the center of the roof (Figure 9b, 9c, and 9d).

It can also be observed from Figures 8 and Figure 9 that the panels act largely independently. For example, Figure 9 shows the strains in the back wall are nearly the same when the module is loaded under only back wall pressure or both back wall and roof pressures. The same is true for the roof when the module is loaded under only roof pressure or both back wall and roof pressures. Therefore, the system could be studied using simplified models of individual panels, an important result that would be applicable in design.

Local behavior was investigated near the roof-wing wall connection (Loc. AI 8, AI 9) and at the wing wall ground restraint (Loc. AO 3) (Figure 10). The numerical models were able to reasonably predict the measured strains at the roof near the roof-wing wall connection (Loc. AI

8). However, the measured behavior in the wing wall at both the roof-wing wall connection (Loc. AI 9) and at the ground restraint (Loc. AO 3) is significantly stiffer than the numerical predictions. This can be attributed to the global translation of the roof (due to the play in the hinges) that would reduce the tensile force imparted in the wing walls, thereby reducing the measured strains. Note that the numerical models were able to accurately predict strains at these locations when only the back wall was loaded (data not shown for conciseness) since the play in the hinges had minimal impact under this loading condition.

Local behavior was also measured near the hinges connecting the wing wall to the back wall (Figure 11). The numerical models provide an excellent match to the measured results under all loading scenarios. Only data for the back wall and roof loading scenarios was shown for conciseness.

Module B Test

Module B, which features a different loading direction on the back wall, was similarly investigated under pressures applied to the back wall, the roof, and both the roof and back wall. A similar effect related to the influence of the play of the hinge connecting the back wall to the roof can be seen in the deformed profile of Module B (Figure 12). Note that a string pot could not be attached to the back wall panel (Loc. BS 1) due to interference with the bladder. The rotation of the roof exhibits the same trend as shown for Module A; however, the numerically predicted strains at the center of the back wall and the center of the roof match well with the measured data (Figure 13). Similar to the Module A results, Figure 13 indicates that the panels act largely independently, thereby offering an opportunity for simplified analysis in a design environment.

Combined Modules Test

Figure 14 shows the measured and numerical deformed shape of Modules A and B when pressure was applied to (a) the back wall and roof of Module A, (b) the back wall and roof of Module B, and (c) the back wall and roof of both Modules A and B. At the roof ridge, there is considerable vertical slip between the two modules. The numerical model over-predicts the magnitude of this slip compared to the measured data. This discrepancy can be attributed to the frictionless contact surface between roof modules in the numerical model, a simplification incorporated in the models since the coefficient of friction between the gasketing at the roof panels was unknown and the magnitude of the clamping force between the modules could not be measured. When the two modules are fully loaded (Figure 14c), the measured and numerical results agree well. This can be attributed to the structure acting as a stiffer, complete unit that minimizes the play in the hinge connecting the back wall and roof. This agreement is further demonstrated in Figure 15 where measured and numerical strains are nearly identical at panel centers under pressures applied to the roof and back wall of Modules A and B.

It can also be observed that when the modules are combined, the back walls continue to act independently (i.e., the strains in the back walls of both Modules A and B during the single module tests when only back wall pressure is applied are nearly the same as during the combined module test when both back wall and roof pressure are applied). However, the strain in the roofs are dramatically reduced when the modules are combined. This is expected since the roof panels change from acting like cantilevers in the single module tests to more of a continuous frame when combined. The relative independence of panel behavior is related to the type of connection between panels. The back walls, which are hinge connected on three sides and are in bearing with the floor on the remaining side, continue to act independently regardless of configuration. However, when the roof panels are connected to one another by clamps, their behavior changes dramatically. This is an important result for design as simplified numerical analyses could be performed to capture system behavior.

Parametric Study of Restraints and Connection between Modules, Gasketing, and Panel Reinforcement

Overall, these comparisons between measured and numerical results for individual and combined modules have culminated in validated numerical models which were used to perform parametric studies investigating the impact of the (1) restraints and the connection between modules, (2) gasketing between panels, and (3) panel end cap reinforcement on system behavior.

To investigate the effect of boundary conditions on the global behavior of the structure, both the roof-to-roof connection and ground restraints were altered (Figure 16a). In addition to the existing horizontal translation restraint at the roof-to-roof connection, restraints in the vertical and out-of-plane direction were added (shown as shear connection at roof). As shown in Figure 16a, these additional restraints remove the relative movement at the roof-to-roof connection and decrease the roof deflections, while minimally affecting the back wall behavior. The existing ground restraints (i.e., fixed restraints on ground angles and flange at bolt locations) were modified to fix the entire bottom of structure (shown as fully fixed restraints). As expected, this created a significant decrease in the overall deflection of the structure. A designer should consider advantages (decreased deflection) and disadvantages (weight, cost, installation) of adding additional restraints.

Gasketing was placed between panels for thermal insulation and waterproofing. As previously mentioned, the gasketing was modeled as an essentially incompressible material. To investigate the impact of the stiffness (i.e., elastic modulus) of the gasketing, the predicted deformed shape from the validated numerical model (i.e., 100% gasketing stiffness) is compared with a numerical model where the gasket stiffness is significantly reduced (to 10% of the stiffness in the validated numerical model). As shown in Figure 16b, the stiffness of the gasketing had a negligible impact on the system behavior. Therefore, a designer should select gasketing based on insulating and waterproofing demands as opposed to compressibility.

To investigate the effect of the reinforced end cap regions on the global behavior of the structure, the end cap regions were removed from all panels (i.e. constant panel face thickness) As shown in Figure 16c, removing these regions slightly increases the deflection of the structure. This is expected, as most of the end cap regions are located at the edges of the panels and, therefore, minimally affect the deflections at the panel centers. As a result, a designer should focus on the local effects (i.e., strains at panel edges and near connections) and weigh the advantages (local stiffening) and disadvantages (cost, weight, manufacturing) when determining the need for panel reinforcement.

CONCLUSIONS

This paper discussed the load-bearing capability of sandwich panels (fiber-reinforced polymer faces and a foam core) connected by aluminum hinges in a deployable structure (Figure 1). The behavior of the structure was measured (1) during deployment, and (2) as both individual and combined modules subjected to uniform surface pressures [emulating wind loads per ASCE/SEI 7-10 design standards (ASCE, 2010)]. The measured results were compared with numerical finite element models. The resulting validated numerical models were then used to perform parametric studies to investigate design decisions for (1) deployment, including panel reinforcement, location of lifting equipment, and size of lifting equipment, and (2) combined modules, including restraints and connections between modules, gasketing between panels, and panel reinforcement.

When investigating the behavior of the system during deployment, the measured and numerical strains of the back wall showed good agreement, with some discrepancy on the left side of the panel that can be attributed to the tightness of fit of the lever arm in the prototype structure. Hand placement on the lever arm (i.e., center, left, or right) had negligible impact on the behavior along the panel midline; however, local strains on the left and right sides were significantly affected. Since hand placement on the lever arm could be unpredictable in field operations, a designer would need to consider an envelope of results. Parametric numerical studies showed that (1) the thickened reinforcement region could be terminated very close to the lever arm attachment, ultimately leading to cost and weight savings, (2) the number of lever arm prongs could be reduced from three to two if sufficient panel reinforcement is provided to withstand the resulting high tensile strains, and (3) a smaller diameter lever arm could be used if sufficient panel reinforcement is provided. A designer would need to weigh the benefits of the reduction in the lever arm prongs and diameter against the added cost and weight of the required additional panel reinforcement.

Measured and numerical results agree well for the individual module and combined module tests. The strains at panel centers agree for all tests, indicating that the numerical models are able to predict the global behavior. Discrepancies in the deformed shape of the individual module tests have been attributed to play in the hinge connecting the back wall with the roof. This difference is also seen in the strains in the wing wall. However, these discrepancies were significantly reduced when the two modules were combined, associated with the greater stiffness of the structure when it forms a complete unit. Measured and numerical results near the hinges connecting the back wall to the wing walls match well. Overall, the numerical models were validated using the measured results and used to perform parametric studies to investigate the impact of the (1) restraints and the connection between modules, (2) stiffness of gasketing, and (3) end cap reinforcement on system behavior. Adding restraints to the roof-to-roof connection decreased the roof displacements, while adding fixed ground restraints substantially decreased the displacement of the entire structure. A designer should weigh these performance advantages with the increased cost, weight, and installation time when determining the connections and ground restraints. A significant reduction in the stiffness of the gasketing showed negligible impact on the behavior of the structure. Therefore, a designer should select gasketing based on insulating/waterproofing needs as opposed to structural demands. Removing the reinforced end cap regions did not have a significant effect on the global behavior of the structure, but could affect local strain behavior. A designer should consider these local effects, as well as the weight and cost, when determining the need for panel reinforcement.

It should be noted that overall the measured strains are low, indicating design conservatism. The FRP layup and the relative thickness of the face and core were designed to meet the limit states of buckling, face stress, core shear stress, shear crimping, and face wrinkling with a safety factor of 1.5, as well as deflection criteria under combined dead, snow, and wind loads. The design of the sandwich panels was governed by panel buckling in the following cases: (1) buckling of the back wall under combined dead and wind loads during deployment and (2) buckling of the roof and wing walls under combined dead, wind, and snow loads as a single, erect module. These analyses were performed using simplified models and conservative estimates of the critical buckling load (Quaglia et al., 2014a). Further research using the validated numerical models in this paper could lead to reduced design conservatism.

Ultimately, this paper demonstrated the load-bearing capability of sandwich panels for deployable structures. It addressed a knowledge gap in the behavior of folding structures comprised of multiple sandwich panels connected by hinges. These studies led to important results for the design of folding structures comprised of multiple sandwich panels. It was observed that the back walls act relatively independently in both the single and combined module tests. Similarly, the roof panels act independently in the single module tests. However, when the roof panels are joined by clasps, their behavior shifts from being cantilever-like to more of a continuous frame. The relative independence of panel behavior is directly related to the type of connection between panels. The back walls continue to act independently regardless of configuration as they are connected to the other panels by hinges on three sides and are in bearing with the floor on the remaining side. Alternatively, when roof panels are connected to one another by clamps, their behavior changes dramatically. These observations would be useful for a broader range of panels and configurations. They are also important for the design of folding structures since simplified numerical models can be used to characterize global behavior.

This research also indicated that the panel-to-panel connections, ground restraints, and the attachment locations for the lever arm are critical elements for design. They are subjected to high, repeated strains under multiple deployments and cyclic loadings. As noted by leading researchers in the field [e.g., De Matteis and Landolfo (1999a), De Matteis and Landolfo (1999b), Demelio et al. (2001), Bunyawanichakul et al. (2005), Heimbs and Pein (2009), Dawood and Peirick III (2013), among others], connections play a major role in sandwich panel behavior and there has been little research dedicated to this topic. Sandwich panels are particularly weak in carrying concentrated loads which occur at these connections (Demelio et al., 2001). Furthermore, there is a lack of efficient strategies for numerically modeling these connections (Bunyawanichakul et al., 2005). Future work is needed investigate failure modes and mitigation strategies of the panel-to-panel connections, ground restraints, and lever arm attachment, including experimental studies leading toward validated numerical modeling strategies.

ACKNOWLEDGMENTS

This material is based upon work supported by the US Army Natick Soldier Research, Development and Engineering Center (NSRDEC) under Contract W911QY-12-C-0128. The authors are grateful for the assistance of laboratory technician Brent Bach and students Chad Quaglia, Casey Casias, Angelene Dascanio, and Jack Reilly. The authors would like to thank Lyman-Morse

Boatbuilding Co. (Thomaston, ME) for manufacturing the prototype. The authors would like to acknowledge the other principal investigators on this project, including Mihir Sen, Panos Antsaklis, Ann-Marie Conrado, and Samuel Paolucci and project coordinators, Patrick Murphy and Mike Zenk. This research was supported in part by the University of Notre Dame Center for Research Computing through computational resources.

REFERENCES

ABAQUS (2013). “ABAQUS/Standard Analysis User’s Manual Version 6.13. Dassault Systemes, Waltham, MA.

Abbadi, A., Koutsawa, Y., Carmasol, A., Belouettar, S., and Azari, Z. (2009). “Experimental and numerical characterization of honeycomb sandwich composite panels.” *Simulation Modelling Practice and Theory*, 17, 1533–1547.

Anderson, S. M. (2011). “Save energy, save our troops. http://www.nytimes.com/2011/01/13/opinion/13anderson.html?_r=0 (June 5, 2014).

ASCE (2010). “Minimum Design Loads for Buildings and Other Structures. *ASCE Standard 7-10*, Reston, VA.

ASTM (2008). “ASTM D3039/D3039M-08: Standard Test Method for Tensile Properties of Polymer Matrix Composite Materials.” ASTM International. West Conshohocken, PA.

ASTM (2010). “ASTM D638-10: Standard Test Method for Tensile Properties of Plastics.” ASTM International. West Conshohocken, PA.

ASTM (2011a). “ASTM C271/C271M-11: Standard Test Method for Density of Sandwich Core Materials.” ASTM International. West Conshohocken, PA.

ASTM (2011b). “ASTM C365/C365M-11a: Standard Test Method for Flatwise Compressive Properties of Sandwich Cores.” ASTM International. West Conshohocken, PA.

ASTM (2011c). “ASTM C393/C393M-11: Standard Test Method for Core Shear Properties of Sandwich Constructions by Beam Flexure.” ASTM International. West Conshohocken, PA.

ASTM (2012). “ASTM D7250/D7250M-06: Standard Practice for Determining Sandwich Beam Flexural and Shear Stiffness.” ASTM International. West Conshohocken, PA.

ASTM (2013). “ASTM D792-13: Standard Test Methods for Density and Specific Gravity (Relative Density) of Plastics by Displacement.” ASTM International. West Conshohocken, PA.

Ballard, Z. C., Thrall, A. P., Smith, B. J., and Casia, C. M. (2016). “Impact of warping and hinged connectors on sandwich panel behavior. ASCE Journal of Structural Engineering, In Press.

Bunyawanichakul, P., Castanie, B., and Barrau, J. J. (2005). “Experimental and numerical analysis of inserts in sandwich panels.” *Applied Composite Materials*, 12(3-4), 177–191.

Charleston Marine Containers, Inc. (2011). “Tricons. http : //www.cmci.com/Tricons.aspx (November 17, 2013).

Clean Seal, Inc. (2015). “Miscellaneous sections. http : //www.cleanseal.com/miscellaneous − sections.html (April 30, 2015).

Compliance Packaging International Ltd. (2013). “463L pallets. http : //www.463lpallet.com/ (June 5, 2014).

Daniel, I. M. and Abot, J. L. (2000). “Fabrication, testing and analysis of composite sandwich beams.” *Composites Science and Technology*, 60(12-13), 2455–2463.

Dawood, M. and Peirick III, L. (2013). “Connection development and in-plane response of glass fiber reinforced polymer sandwich panels with reinforced cores.” *Canadian Journal of Civil Engineering*, 40(11), 1117–1126.

De Matteis, G. and Landolfo, R. (1999a). “Mechanical fasteners for cladding sandwich panels: Interpretative models for shear behaviour.” *Thin-Walled Structures*, 35(1), 61–79.

De Matteis, G. and Landolfo, R. (1999b). “Structural behaviour of sandwich panel shear walls: An experimental analysis.” *Materials and Structures*, 32(219), 331–341.

Demelio, G., Genovese, K., and Pappalettere, C. (2001). “An experimental investigation of static and fatigue behavior of sandwich composite panels joined by fasteners.” *Composites Part B: Engineering*, 32(4), 299–308.

El-Chiti, F. (2005). “Experimental variability of e-glass reinforced vinyl ester composites fabricated by vartm/scrimp.” M.S. thesis, University of Maine, Orono, ME.

Gurit (2013). “Corecell M-foam - the marine foam. $http://www.gurit.com/files/documents/corecell - m - foamv5pdf.pdf$ (October 9, 2013).

Heimbs, S. and Pein, M. (2009). “Failure behavior of honeycomb sandwich corner joints and inserts.” *Composite Structures*, 89(4), 575–588.

Kee Paik, J., Thayamballi, A. K., and Kim, G. S. (1999). “Strength characteristics of aluminum honeycomb sandwich panels.” *Thin-Walled Structures*, 35(3), 205–231.

Kesler, O. and Gibson, L. J. (2002). “Size effects in metallic foam core sandwich beams.” *Materials Science and Engineering A*, A326, 228–234.

Malcom, A. J., Aronson, M. T., Deshpande, V. S., and Wadley, H. N. G. (2013). “Compressive response of glass fiber composite sandwich structures.” *Composites Part A: Applied Science and Manufacturing*, 54, 88–97.

Mamalis, A. G., Manolakos, D. E., Ioannidis, M. B., and Papapostolou, D. P. (2005). “On the crushing response of composite sandwich panels subjected to edgewise compression: Experimental.” *Composite Structures*, 71(2), 246–257.

Manalo, A. C., Aravinthan, T., Karunasena, W., and Islam, M. M. (2010). “Flexural behaviour of structural fibre composite sandwich beams in flatwise and edgewise positions.” *Composite Structures*, 92(4), 984–995.

Martinez-Martin, F. J. and Thrall, A. P. (2014). “Honeycomb core sandwich panels for origami-inspired deployable shelters: multi-objective optimization for minimum weight and maximum energy efficiency.” *Engineering Structures*, 69, 158–167.

Peraza-Hernandez, E. A., Hartl, D. J., Malak Jr., R. J., and Lougads, D. C. (2014). "Origami-inspired actives structures: a synthesis and review." *Smart Materials and Structures*, 23(9), 094001.

Quaglia, C. P., Dascanio, A. J., and Thrall, A. P. (2014a). "Bascule shelters: A novel erection strategy for origami-inspired structures." *Engineering Structures*, 75, 276–287.

Quaglia, C. P., Yu, N., Thrall, A. P., and Paolucci, S. (2014b). "Balancing energy efficiency and structural performance through multi-objective shape optimization: Case study of a rapdily deployable origami-inspired shelter." *Energy and Buildings*, 82, 733–745.

Russo, A. and Zuccarello, B. (2006). "Experimental and numerical evaluation of the mechanical behaviour of GFRP sandwich panels." *Composite Structures*, 81(4), 575–586.

The Aluminum Association (2005). "Aluminum Design Manual: Specifications & Guidelines for Aluminum Structures. USA.

United States Army Integrated Logistics Support Center Natick (2013). "Force Provider. http://ilsc.natick.army.mil/forceprovider.htm (November 17, 2013).

Vectorply (2002). "Laminated properties and packaging. http://www.vectorply.com/ri-laminateprop.html (November 29, 2014).

List of Tables

TABLE 1: Measured material properties of sandwich panel components, reprinted from Ballard et al. (2016).

	Panel Core					Panel Face			
Property	ρ_c (kg/m^3)	E_c (MPa)	σ_c (MPa)	τ_c (MPa)	G_c (MPa)	ρ_f (kg/m^3)	E_f (MPa)	σ_f (MPa)	ν_f
Mean	87.5	57.7	1.25	1.56	47.2	1740	15500	283	0.261
Std. Dev.	0.833	2.44	9.86e-3	9.45e-3	2.16	5.20	737	17.0	0.0145
COV	0.950%	4.23%	0.790%	6.03%	4.59%	0.299%	4.76%	6.02%	5.55%
ASTM Standard	C271	C365		C393	D7250	D792	D3039		
No. of Samples	10	10	10	5	5	5	8	5	8

Note: Subscripts c and f correspond to sandwich panel core and face, respectively. ρ = density, E = elastic modulus, σ = ultimate strength, τ = shear strength, G = shear modulus, ν = Poisson's ratio, Std. Dev. = standard deviation, and COV = coefficient of variation.

TABLE 2: Prototype connection details.

Detail Type	Relevant Details
A. Hinge	Open leaf width: 76.2 mm (3.0 in), length: 76.2 mm (3.0 in), thickness: 2.54 mm (0.100 in), pin diameter: 6.35 mm (0.250 in)
B. Cont. Hinge	Open leaf width: 76.2 mm (3.0 in), length: 1070 mm (42.0 in), thickness: 2.54 mm (0.100 in), pin diameter: 6.35 mm (0.250 in)
C. Gasketing	Ethylene propylene diene monomer rubber, Clean Seal Product 50500 (Clean Seal, Inc., 2015)
D. Ground Angle	Width: 50.8 mm (2.00 in), height: 50.8 mm (2.00 in), length: 152 mm (6.00 in), thickness: 3.18 mm (0.125 in)
E. Flange	Length: 44.5 mm (1.75 in), thickness: 6.35 mm (0.250 in)
F. Roof Angle	Width: 38.1 mm (1.50 in), height: 38.1 mm (1.50 in), length: 102 mm (4.00 in), thickness: 3.18 mm (0.125 in)

List of Figures

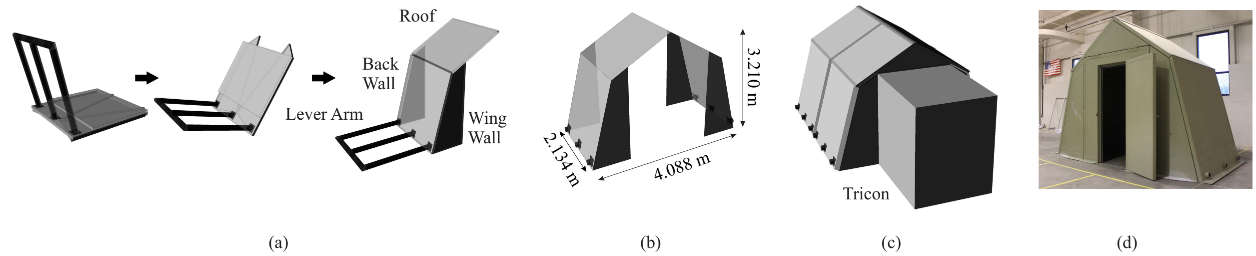

FIG. 1: Origami-inspired deployable shelter developed by Quaglia et al. (2014a): (a) deployment, (b) two modules with dimensions, (c) complexed, enclosed modules with a Tricon container, and (d) full-scale deployed prototype. Images (a)-(c) reprinted from Ballard et al. (2016).

(a) (b) (c) (d)

FIG. 2: Samples for material testing: (a) core, (b) FRP face, (c) dog-bone FRP face, and (d) sandwich panel.

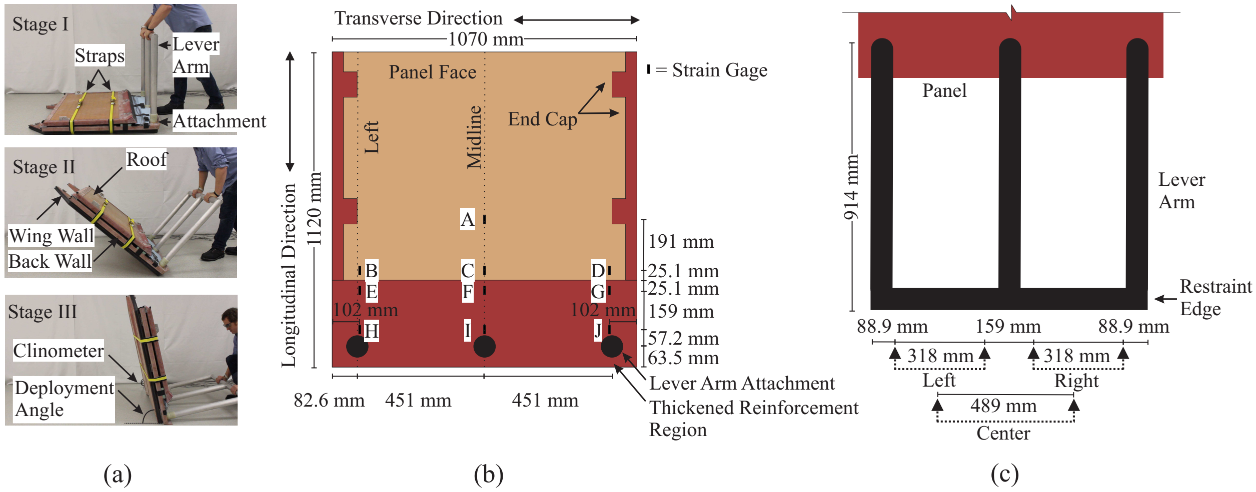

FIG. 3: Deployment test: (a) photograph, (b) plan view of measurement system on back wall, and (c) plan view of varying hand positions on lever arm.

FIG. 4: Module A test: (a) elevation view, (b) photograph, and (c) isometric view; Module B test: (d) elevation view, (e) photograph, and (f) isometric view; Two Module test: (g) elevation view, (h) photograph, and (i) isometric view; Photographs of connection details: (j) ground restraints for wing walls and back walls, (k) connection between wing wall and roof, and (l) roof connection between modules.

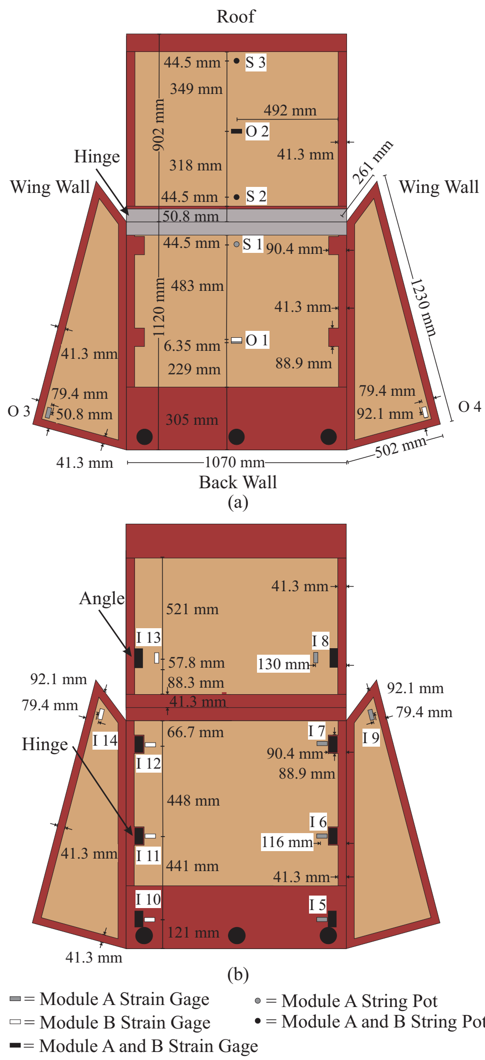

FIG. 5: Module tests: plan view of measurement system shown in a flat (i.e., undeployed) configuration on the (a) outside, and (b) inside surfaces.

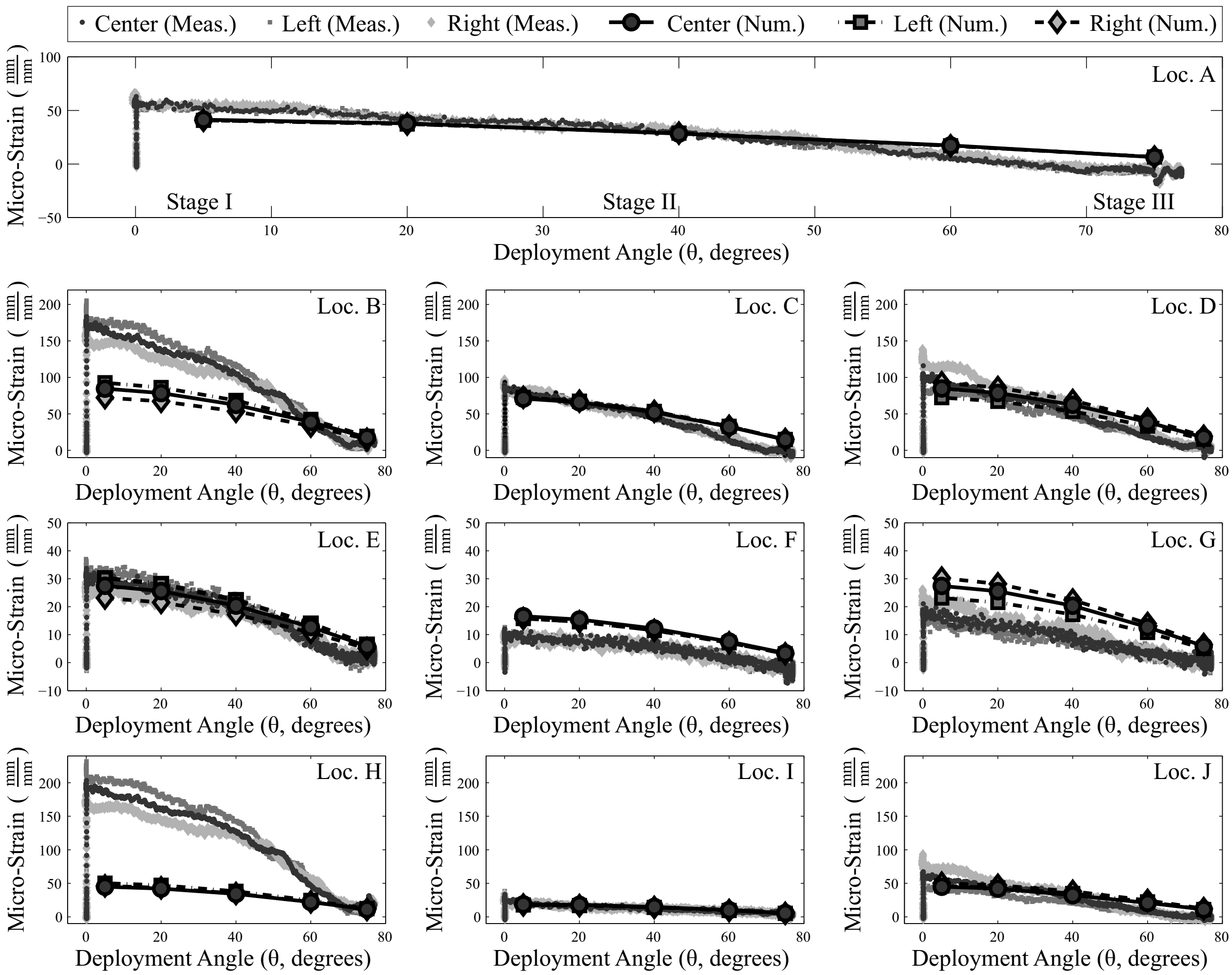

FIG. 6: Measured and numerical longitudinal surface strains during deployment for hand positions at center, left, and right on lever arm.

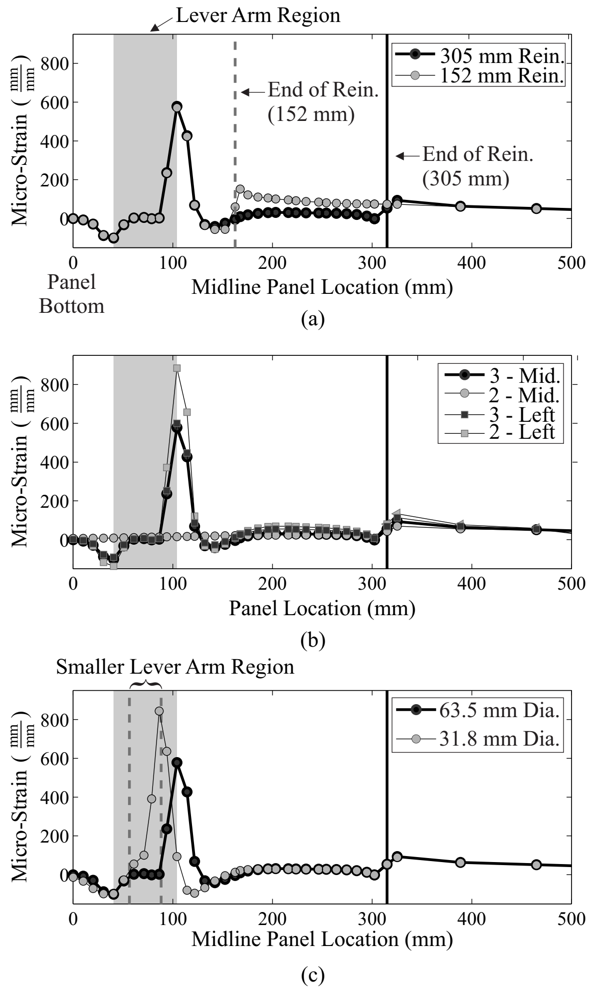

FIG. 7: Impact of (a) length of reinforcement region, (b) number of lever arm attachments, and (c) diameter of lever arm on behavior during deployment: Numerical longitudinal surface strains at deployment angle $\theta = 5°$ along longitudinal length of panel.

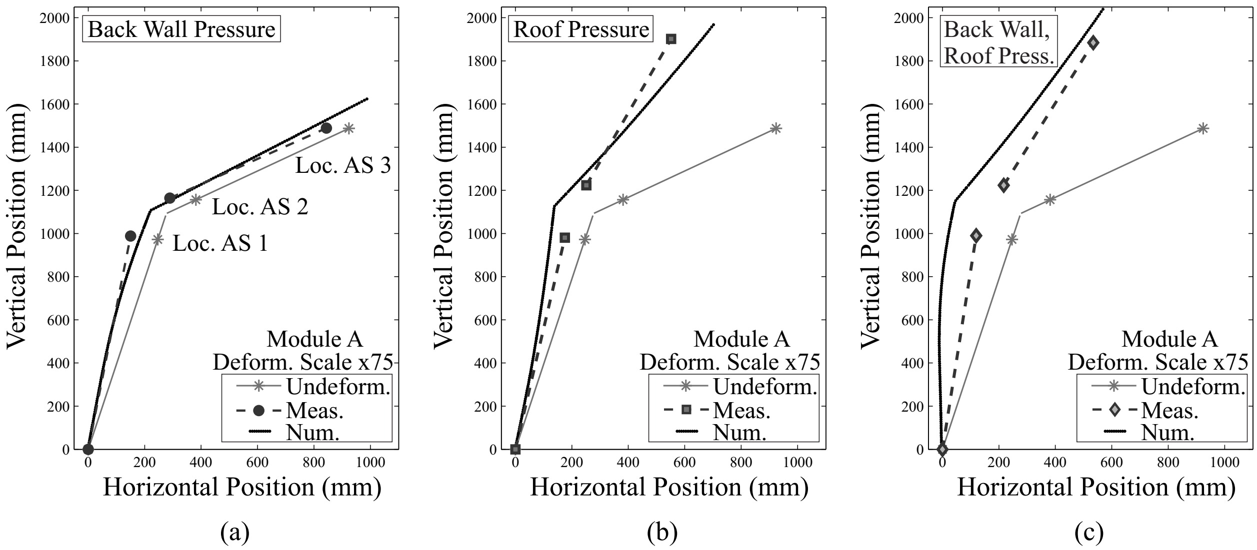

FIG. 8: Module A test: measured and numerical deformed profiles for pressures applied to (a) back wall, (b) roof, and (c) back wall and roof, compared against the undeformed (undeform.) shape. Measured data is connected by dashed, straight lines for reference and deformations are multiplied by scale factor of 75 for clarity.

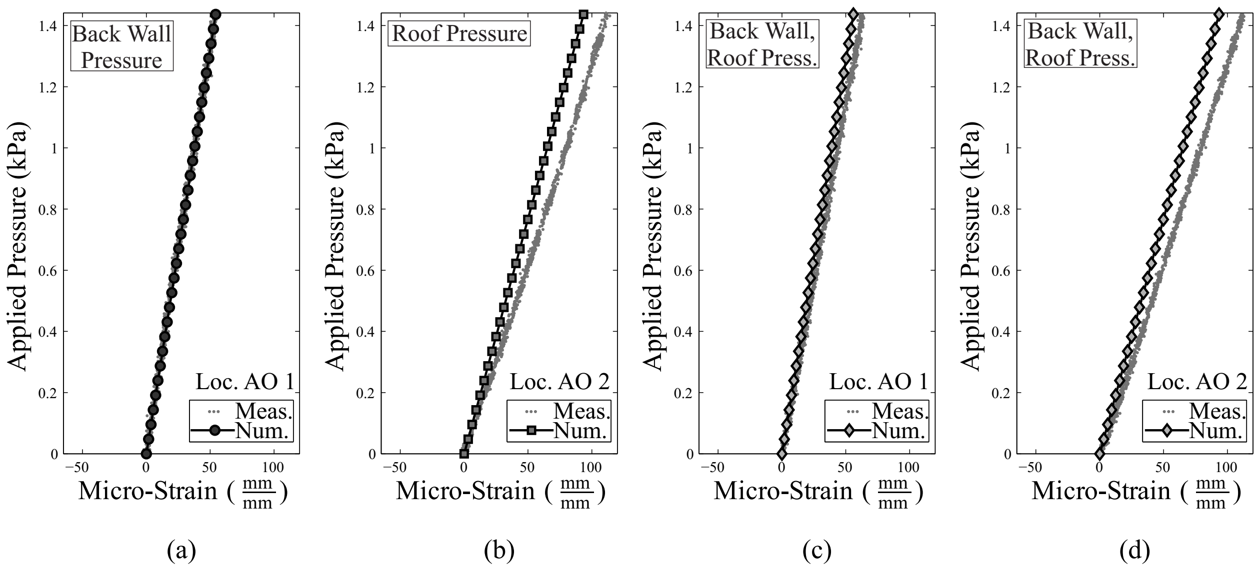

FIG. 9: Module A test: measured and numerical surface strains for pressures applied to (a) back wall (strain at center of back wall), (b) roof (strain at center of roof), (c) back wall and roof (strain at center of back wall), and (d) back wall and roof (strain at center of roof).

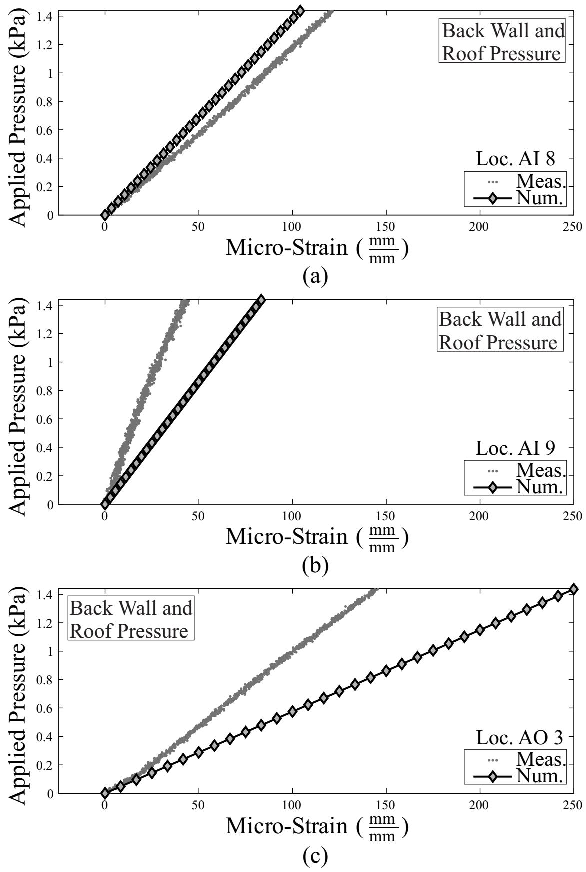

FIG. 10: Module A test: measured and numerical surface strains at (a) roof near roof-wing wall connection, (b) at wing wall near roof-wing wall connection, and (c) and at wing wall near ground restraint when pressure applied to back wall and roof simultaneously.

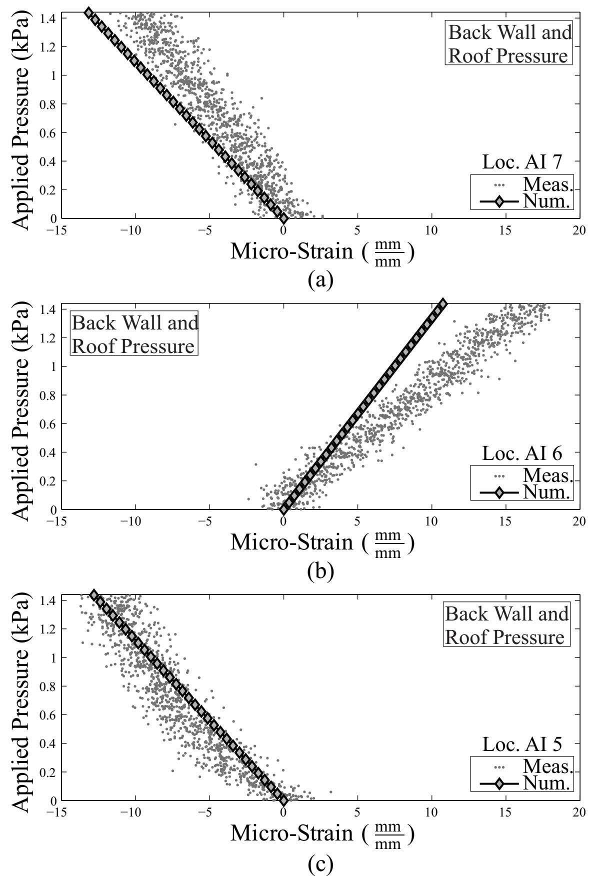

FIG. 11: Module A test: measured and numerical surface strains at back wall for pressure applied to the back wall and roof at (a) top hinge, (b) middle hinge, and (c) bottom hinge.

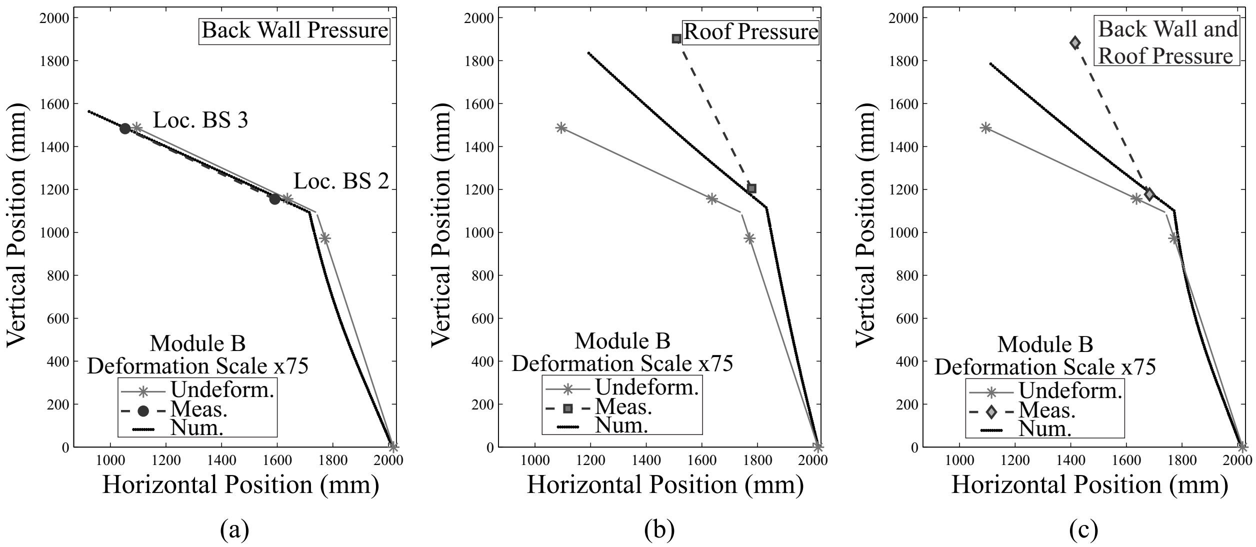

FIG. 12: Module B test: measured and numerical deformed profiles for pressures applied to (a) back wall, (b) roof, and (c) back wall and roof, compared against the undeformed (undeform.) shape. Measured data is connected by dashed, straight lines for reference and deformations are multiplied by scale factor of 75 for clarity.

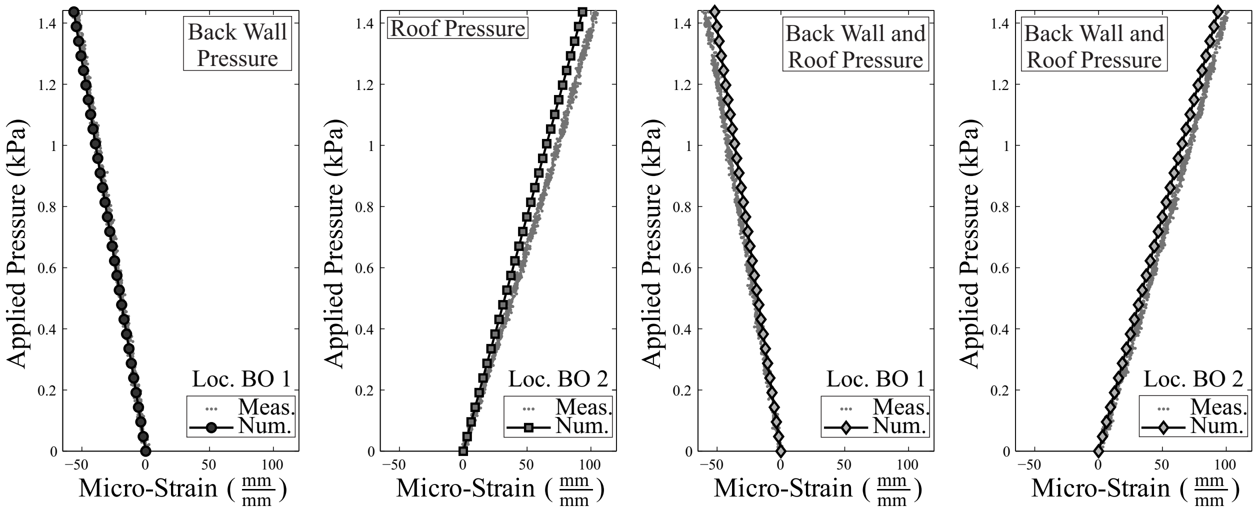

(a) (b) (c) (d)

FIG. 13: Module B test: measured and numerical surface strains for pressures applied to (a) back wall (strain at center of back wall), (b) roof (strain at center of roof), (c) back wall and roof (strain at center of back wall), and (d) back wall and roof (strain at center of roof).

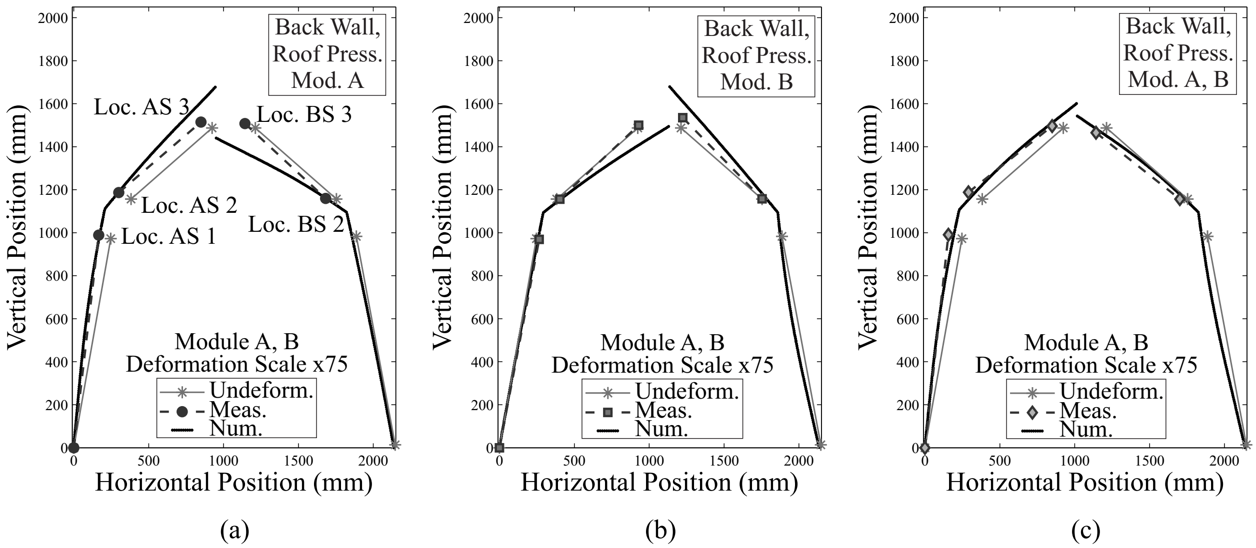

FIG. 14: Two Module test: measured and numerical deformed profiles for pressures applied to (a) back wall and roof of Module A, (b) back wall and roof of Module B, and (c) back wall and roof of both Modules A and B, compared against the undeformed (undeform.) shape. Measured data is connected by dashed, straight lines for reference and deformations are multiplied by scale factor of 75 for clarity.

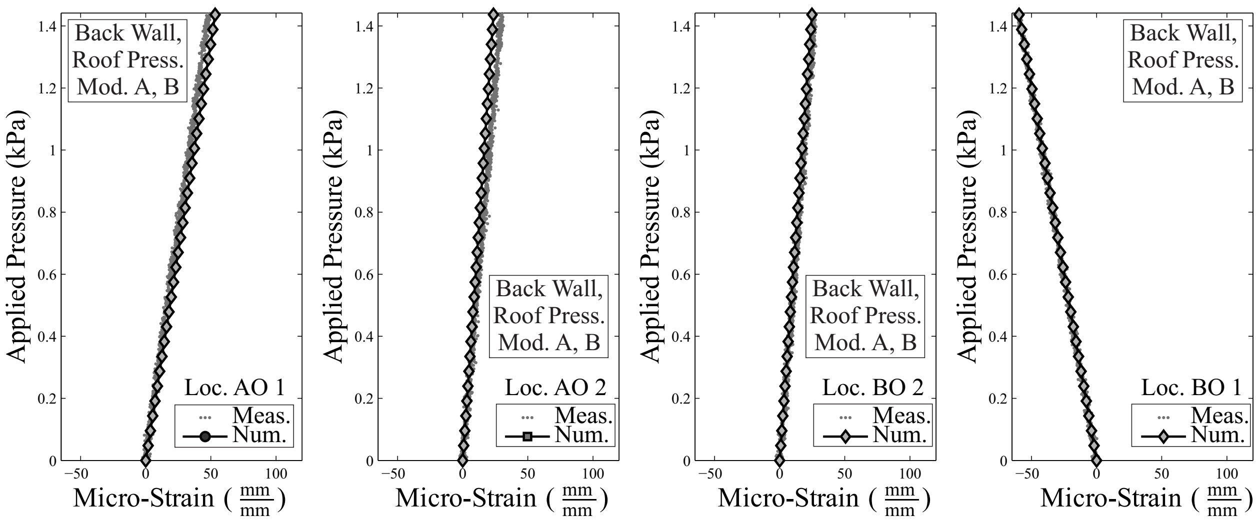

(a) (b) (c) (d)

FIG. 15: Two Module test: measured and numerical surface strains for pressures applied to back wall and roof of both Modules A and B at (a) center of back wall of Module A, (b) center of roof of Module A, (c) center of roof of Module B, and (d) center of back wall of Module B.

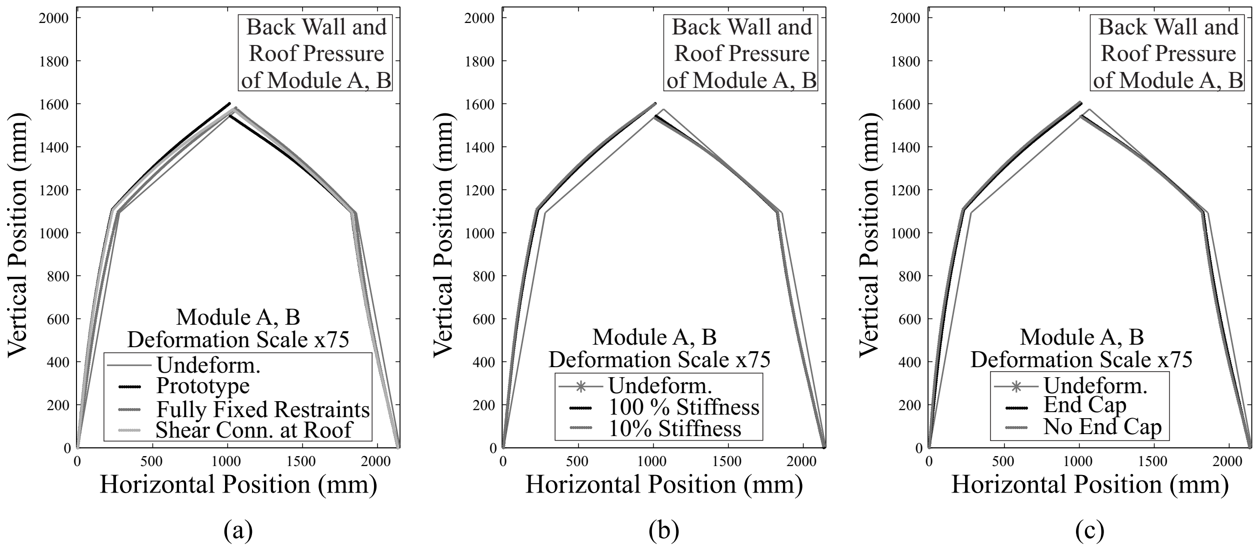

FIG. 16: Impact of (a) restraints and the connection between modules, (b) stiffness of gasketing, and (c) end cap reinforcement on deformed shape for pressures applied to back wall and roof of both Modules A and B. Deformations are multiplied by scale factor of 75 for clarity.